PCCP

PAPER

View Article Online
View Journal | View Issue

Cite this: *Phys. Chem. Chem. Phys.*, 2015, **17**, 12812

Two-dimensional electron gas and its electric control at the interface between ferroelectric and antiferromagnetic insulator studied from first principles

Vladislav Borisov,*[ab] Sergey Ostanin[b] and Ingrid Mertig[ab]

Received 12th December 2014,
Accepted 7th April 2015

DOI: 10.1039/c4cp05831c

www.rsc.org/pccp

A multiferroic interface between the antiferromagnetic Slater insulator $SrTcO_3$ and ferroelectric $BaTiO_3$ (BTO) is studied from first principles. Although the interfacial magnetoelectric coupling of $SrTcO_3$(001) is relatively small, we found that a two-dimensional electron gas (2DEG) appears for both BaO/TcO_2 and TiO_2/SrO terminations. The charge character of the carriers, induced in the band gap due to polar BTO, can be switched from electrons to holes by the reversal of the electric polarization in BTO. The 2DEG is robust and stable against the degree of electronic correlations, whereas the paraelectric state of BTO suppresses the 2DEG. The origin of the 2DEG at the $BTO/SrTcO_3$ interface and its key factors are discussed.

1 Introduction

The interfaces between insulating oxides can behave exotically. For instance, the observation of a two-dimensional electron gas (2DEG) in $LaAlO_3/SrTiO_3$ (LAO/STO), which is discussed usually in the context of its LaO/TiO_2-terminated interface, is one of the most fascinating examples.[1–4] Until now, the nature of the 2DEG in LAO/STO has not been completely understood, although a few scenarios were suggested in the literature, which include: (i) the oxygen vacancy-induced mechanism,[5] (ii) the La/Sr interfacial mixing[6] and, finally, (iii) the defectless electronic reconstruction which manifests itself as a charge transfer into the Ti t_{2g} orbitals, and subsequently, the formation of mixed valence states and charge/orbital ordering at the LaO/TiO_2-terminated interface.[7] In view of the most recent experimental findings regarding the different interfacial morphologies and non-equilibrium LAO/STO structures,[8] the focus of discussions around the 2DEG phenomenon might shift to the intrinsic properties of the TiO_2-terminated interface.

When the $SrTiO_3$ component of the 2DEG composite system is replaced by a robust ferroelectric (FE), such as $BaTiO_3$ (BTO), this may create an extra functionality due to its switchable polarization. Indeed, the LAO/BTO heterostructure has been recently fabricated.[9] In general, the interplay between the electronic and structural properties seen at the interface between ferroelectrics and metals (or gapless oxides) has been well understood during the last decade.[10,11] For the FE–ferromagnet composite multiferroics, when magnetoelectric coupling is strong enough the switching of the magnetization by an external electric field might be realized.[12,13] In principle, the change of magnetization, ΔM, induced by the FE polarization reversal can be crudely estimated[12] using the coercive field E_c: $\Delta M \sim \alpha E_c$, where α is the magnetoelectric coupling (MEC) coefficient. Concerning the multiferroic interfaces calculated from first principles, the effect of a magnetically ordered oxide on the 2DEG was studied so far using the superlattice geometry.[14]

Meanwhile, among all magnetically ordered oxides, the overwhelming majority are antiferromagnetic (AFM), which vary considerably in their electronic and temperature-dependent magnetic properties. In principle, some AFM perovskites ABO_3 can be combined with robust ferroelectrics, such as BTO, in a reasonably good lattice match and, therefore, the AFM/FE oxide interfaces can be grown epitaxially. When the 3d cation occupies the B site of ABO_3 the compound usually shows ferromagnetism. For example, this happens in $SrCoO_3$ with a Curie temperature (T_C) of 280 K, not far below room temperature but, unfortunately, below the needed window of ferroelectric functionality. All experimental data widely presented in the literature indicate that, in contrast to 3d perovskites, the compounds with 4d or 5d cations on the B site display a less tendency to magnetism. This is due to their spatially extended 4d (5d) orbitals compared to those of 3d perovskites.[15,16]

In this work, we suggest the use of recently synthesized $SrTcO_3$ for the multiferroic $BaTiO_3/SrTcO_3$ interface. According to the available experimental data,[17,18] $SrTcO_3$ is antiferromagnetic, whose surprisingly high Néel temperature is $T_N \rightarrow 1000$ K and the Tc magnetic moment equals 1.87 μ_B measured at room

[a] *Institute of Physics, Martin Luther University Halle-Wittenberg, Von-Seckendorff-Platz 1, 06099 Halle, Germany. E-mail: vladislav.s.borisov@gmail.com*
[b] *Max Planck Institute of Microstructure Physics, Weinberg 2, 06120 Halle, Germany*

temperature. The compound possesses an orthorhombically distorted perovskite structure with *Pnma* symmetry where the Tc nearest neighbors are ordered antiferromagnetically, thereby forming the G-type AFM configuration similar to that seen in $SrMnO_3$.[15] The average Tc–Tc distance is 3.976 Å. Therefore, for the BTO/$SrTcO_3$(001) interface the lattice mismatch is less than 1%, which allows epitaxial growth. It was suggested[17] that the anomalously high T_N of $SrTcO_3$ is due to the particularly strong covalency of Tc–O bonds. The corresponding first-principles calculations[17,19,20] demonstrate the electronic hybridization between the Tc 4d states and oxygen 2p states close to the top of the valence band. The calculated T_N, which is in a good agreement with the experimental data,[17,18] increases with an increase in volume, whereas the presence of vacancies on both the oxygen and cation sites of $SrTcO_3$ should significantly suppress the critical temperature, as well as the magnetic moment of Tc.[20] Electronic correlations play a minor role in the formation of the magnetic state, although they improve the calculated value of T_N. Until now, the experimental band gap value of $SrTcO_3$ has not been available. However, the *ab initio* calculations of $SrTcO_3$, which use the moderate Hubbard parameter and which yield simultaneously the optimal set of all magnetic properties including T_N, suggest that the band gap is <0.5 eV.[20] From this point of view, $SrTcO_3$ might be considered as an antiferromagnetic semiconductor rather than an insulator when the corresponding tunnel barrier is studied.

Here, we computed the structural, magnetic and electronic properties of BTO/$SrTcO_3$(001) focusing on how the proximity of the two ferroics changes the electronic states near the Fermi level. The paper is organized as follows: in Section II we describe the structure model and give the essential details of our *ab initio* calculations. The relaxed atomic positions near the interface and their influence on intrinsic antiferromagnetism of $SrTcO_3$ are analyzed in Section III. Here, we discuss the geometry of the oxygen octahedra and the cation–oxygen bonds in connection with the chemical environment of the interface. In Section IV, we focus on the electronic states, which are localized on interfacial cations and which appear near the Fermi level due to the charge transfer. The effect of strong electronic correlations is studied within the Hubbard parametrization. The 2DEG effect is illustrated by the local density of states and a quasi-two-dimensional band structure. Finally, we give a summary of our *ab initio* study and discuss some important implications.

2 Details of calculations

The calculations were performed using the Vienna Ab initio Simulation Package (VASP),[21–23] within the generalized-gradient approximation (GGA) to the exchange–correlation potential.[24] The electron–ion interactions were described by projector-augmented wave pseudopotentials,[25] and the electronic wave functions were represented by plane waves with an energy cutoff of 460 eV. For ionic relaxation, the Γ-centered $(4 \times 4 \times 2)$ k-point Monkhorst–Pack[26] mesh was used. After relaxation the calculated forces are always less than 1×10^{-2} eV Å^{-1}. The use of a more dense k-mesh yields essentially the same atomic positions. For the density of states (DOS), the tetrahedron method and the $8 \times 8 \times 2$ k mesh were utilized with no smearing. To take into account the effect of strong electronic correlations, the GGA + U parametrization[27] was applied on the 4d orbitals of technetium. The U parameter, which is in this context an adjustable parameter, is ranging between $U = 0$ and 3 eV, including $U = 0.5$ eV, which was optimized previously for bulk $SrTcO_3$.[20] By comparing results for different values of U with those for $U = 0$ one can conclude on the importance of the correct band gap of $SrTcO_3$ for the formation and density of the 2DEG. In addition, the effect of the BTO band gap is studied for one interface configuration using GGA + U with $U = (0–8)$ eV applied on the Ti d states.

The analysis of *ab initio* calculations published so far on LAO/STO[1–8] shows that the structural model has been transformed from the initially used superlattice to the slab geometry with a vacuum layer, which separates the two insulating materials. The latter approach allows to confirm, for instance, the thickness-dependent transition from the insulating state of LAO/STO to the 2DEG behavior.[2,28] The Hubbard U-parametrization is used then to model the mixed-valency state of Ti at the interface within the slab option.[28] One can argue that the slab with vacuum leads to incorrect electrostatic boundary conditions for the studied interface. This refers to a long-standing problem of polar discontinuity. The use of the superlattice removes the most serious questions concerning the electrostatic boundary conditions. Thus, it would be worthwhile to use the two structural models and compare their results.

Regarding composite ferroelectrics, it is experimentally established that BTO films grow in complete unit cells on an atomically clean substrate.[29] For that reason, the interface between $BaTiO_3$ and $SrTcO_3$ can be dually terminated, namely, either TiO_2/SrO (TiS) or BaO/TcO_2 (BT). In our work, these two terminations were simulated separately within the supercell with vacuum (SwV), whereas the use of superlattice (SL) mimics the terminations TiS and BT simultaneously as shown in Fig. 1b. For the SL model, its supercell combines 5-u.c. thick BTO and 7-u.c. thick $SrTcO_3$ stacked along the [001] direction, as shown in Fig. 1. In the case of SwV, we took 8 u.c. of $SrTcO_3$ and 5 u.c. of $BaTiO_3$ while a vacuum layer of 17 Å is added to prevent spurious interactions between the periodic images. In all calculations, each planar (x,y)-layer contains two formula units to adopt the AFM ordering and tilting patterns of oxygen octahedra seen in $SrTcO_3$. The chosen thickness of $SrTcO_3$ was found to be thick enough to separate the interface from the free surface in the SwV model, and the two interfaces from each other in our SL model. The in-plane lattice parameter was fixed to the experimental value of bulk $BaTiO_3$ (a_0 = 3.991 Å) to simulate the epitaxial growth of $SrTcO_3$ on the ferroelectric substrate. According to the recent experimental data,[17] the lattice parameter of $SrTcO_3$ is 3.976 Å, which, in view of the larger lattice constant of BTO, may lead to a moderate tetragonal contraction along [001] of about 0.5%. Our GGA-PBE calculations give a similar result: the estimated equilibrium

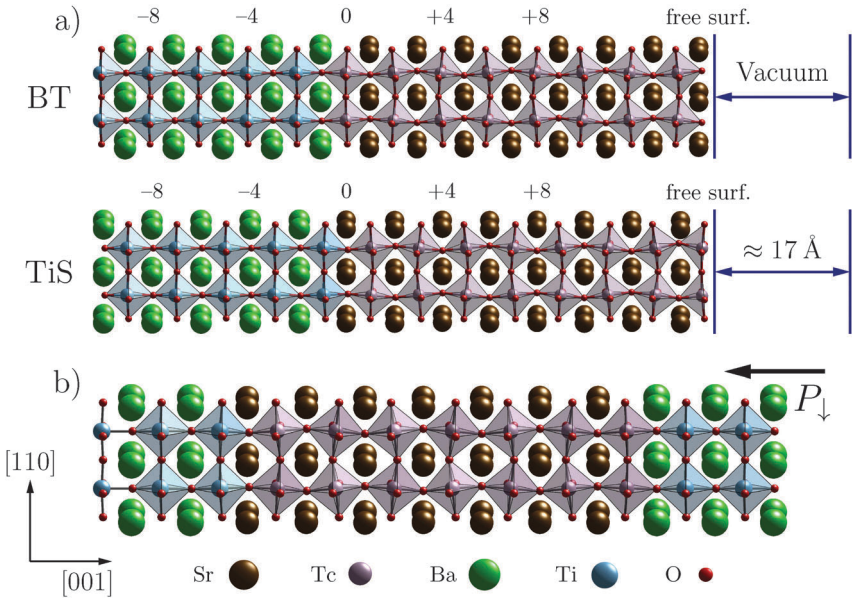

Fig. 1 The side view of the supercell with vacuum (a) and without vacuum, *i.e.* the superlattice (b), both of which were used to model the $BaTiO_3$/$SrTcO_3$(001) interface. Here, the two different interfaces, BaO/TcO_2 and TiO_2/SrO, are marked as BT and TiS, respectively. The numeration of atomic layers outward the interface, as shown in the panel (a), together with the abbreviation for the interface type is used throughout all figures and also for the superlattice to address a particular atomic layer. The electric polarization of $BaTiO_3$ is oriented along the [001] direction while the case of $P_\downarrow$ is shown by the horizontal arrow in panel (b).

lattice constants equal approximately 4.04 Å and 3.98 Å for BTO and $SrTcO_3$, respectively, meaning, similar to the experiment, that a tetragonal deformation of the magnetic oxide is anticipated in this structure.

In our SwV calculations, the two most distant BTO unit cells from the interface were fixed during relaxation to keep a certain polarization state, while all other ions were allowed to relax. In the superlattice, the three central unit cells of each oxide were fixed and all other atoms were relaxed, but when we allowed all BTO ions to relax their coordinates were almost the same. It should be noted that BTO films thinner than 5 unit cells are ferroelectrically unstable and the depolarization effect takes place, in accordance with the recent findings.[10,12,30] In this work, we do not focus on the BTO free surface and the depolarization field effect. Although the intralayer cation–oxygen displacements may be detected in ultrathin BTO films of $n < 4$,[31] such films are not ferroelectric. Some authors suggest that the critical thickness of a robust FE film might be about 10 nm.[32–35] The discussion goes beyond the scope of our study. Instead, we model the polarization reversal in BTO using relatively thin slabs and the scheme described in ref. 36. Thus, one can construct the two dually polar supercells corresponding to $P_\downarrow$ and $P_\uparrow$, in which the BTO part contains at least 5 unit cells where the ionic displacements in each atomic layer were fixed before relaxation to the bulk values. For the polarization state $P_\downarrow$, we place oxygen atoms above the cations in each layer, and *vice versa*, the state $P_\uparrow$ means that all intralayer displacements $\Delta z = z_{cation} - z_O > 0$. Additionally, the paraelectric state of BTO ($P = 0$) was calculated starting from zero intralayer ionic displacements $\Delta z = 0$. After relaxation we compared the structural changes, which occur near the two chemically different interfaces, referred below as TiS and BT. Most important, in this context, is to know whether the existence of electric polarization and/or its direction affect the electronic states at the interfaces. For each polarization, the energies of all possible magnetic configurations of $SrTcO_3$, namely the G-, C- and A-type AFM ordering,[18] were collected for comparison. Below, presenting the results obtained within the SwV model, we always compare them with those of the SL model to reveal their major similarities.

3 $BaTiO_3$/$SrTcO_3$ interfaces

3.1 The relaxed structure

Chemical bonding at the TiS and BT interfaces is mediated by oxygen atoms placed in the layers TiS and (BT-1) atop Ti and Tc, respectively, as shown in Fig. 1. Both the SL and SwV models suggest that the interfacial Ti–O and Tc–O separations are rather sensitive to the **P**-reversal of BTO since the change of the corresponding bond lengths is about 9% (see Table 1). Such large variations affect the strength of the orbital hybridization and exchange interactions at the interface. Paraelectric BTO results in the interfacial bond lengths whose values are varied

Table 1 Relaxed Ti–O and Tc–O separations at the TiS and BT interfaces for the three polarization states, simulated within the SwV model

	Termination	$P_\downarrow$	$P = 0$	$P_\uparrow$
Ti–O (Å)	TiS	2.04	1.95	1.90
	BT	2.16	2.01	1.93
Tc–O (Å)	TiS	1.96	2.01	2.02
	BT	2.00	2.07	2.10

between those of the two polar states, $P_\uparrow$ and $P_\downarrow$. The BT termination shows stronger changes upon the **P**-reversal, as compared to TiS.

To demonstrate the structural changes occurring in BTO near the interface one can use the intralayer cation–oxygen displacements along [001], which visualize the depolarization effect. These Δz values were calculated as the average z-coordinate separation between the Ti/Ba cations and oxygen atoms. In bulk BTO for its optimized tetragonal elongation $c/a = 1.013$, the corresponding ionic displacements are $\Delta_{Ti-O} = 0.13$ Å and $\Delta_{Ba-O} = 0.10$ Å. At the interfaces, the relaxed Δz values are reduced for $P_\uparrow$, especially in the TiS case, which happens because of the local metallization of BTO, as we will see further. For the opposite polarization, Δz values are almost the same as in the bulk (Fig. 2). The SL model shows similar trends. Moreover, when we force the initial BTO displacements to be zero (the case $P = 0$), the relaxation results in notably distinct and negative Δz within the first two u.c. near the interface. This can be understood as an effect of the interface dipole that forms in this system in order to screen the abrupt potential change across the interface, which is itself determined by the band alignment in the two materials. In the studied case, as our results indicate, moderate ionic displacements ≈ 0.05 Å are sufficient to provide an effective screening. Such a behavior might be important when a 2DEG is formed, especially in view of the fact that the interface dipole alone is responsible for the 2DEG observed in semiconductors. In oxides, similar distortions with $\Delta z \neq 0$ were found, for instance, in the $LaAlO_3/SrTiO_3(001)$ heterostructure (see Fig. 2 in ref. 28) which reflects the tendency of the lattice to screen the excess charge due to the polar catastrophy mechanism. In our case, however, the excess charge would be due to the $BaTiO_3$ polarization and a partial screening of this charge can be achieved through ferroelectric-like displacements in $SrTcO_3$.

Regarding the tilting pattern of $SrTcO_3$, all relaxed O octahedra, seen near the interfaces and (001) surfaces, tend to be less rotated compared to the bulk material. It should be noted here that each TcO_2 layer of the supercell contains two Tc and, accordingly, there are two pairs of altered Tc–O–Tc angles, Θ. In bulk $SrTcO_3$, all Θ values are the same: $\Theta = 167.4^\circ$. However, near the interface and surface the altered-angle values of each pair become slightly different and, therefore, we used the average $\langle\Theta\rangle$ in Fig. 2 to characterize the tilting degree. For the $SrTcO_3(001)$ surface, the illustration and details are given in Appendix A (Fig. 13). In general, among the four Θ's there are two types that differ from each other. This is due to BTO, which breaks the Pnma symmetry of $SrTcO_3$, so that the alternating tilting angles are deformed differently near the interface. For the TiS termination, (i) the tilting variation is not sensitive to the polarization reversal, and (ii) the interfacial $\langle\Theta\rangle$ is increased by almost 9° over the bulk value and, then, outward the interface $\langle\Theta\rangle$ quickly approaches its bulk value. For the other interface, BT, we found that the interfacial tilting is significantly suppressed ($\Theta \rightarrow 180^\circ$) while the polarization reversal of BTO yields a minor effect. Such tilting variations were reproduced using the superlattice and, hence, both structural models suggest that the tilting flattens within a couple of unit cells near the interface. In Appendix A, we show also the flattening near the $SrTcO_3(001)$ surface (Fig. 15). The Tc layers, which are distant from both the interface and the surface, are characterized by the uniform distribution of their tilting angles whose values are close to that of bulk $SrTcO_3$.[17]

As we noted before, the structural changes may affect the exchange interactions and magnetic ordering near the $SrTcO_3$ interface. The relation between structure and magnetism has been recently discussed for the 4d $ATcO_3$ family.[19,37] Our results also show that the magnetic moments of the AFM-ordered Tc cations can be tuned near the interface by the BTO polarization reversal, although the overall magnetic symmetry appears to be robust. This issue is discussed below.

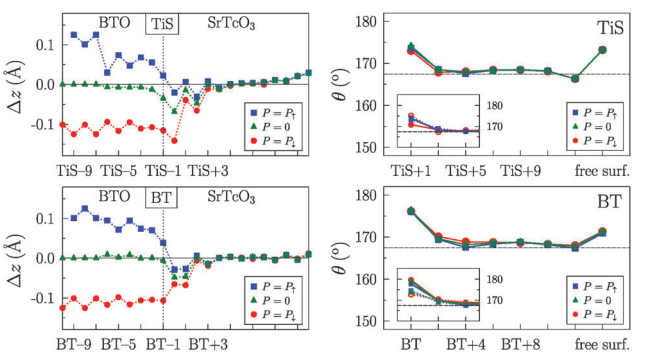

Fig. 2 The relaxed layer-resolved ionic displacements Δz (left panels) and the Tc–O–Tc tilting angles, Θ, (right panels) plotted *vs.* the layer position outward the interface for the three P-states: $P_\downarrow$, $P = 0$ and $P_\uparrow$. The topmost BTO layer near the TiS (BT) interface is shown by a dashed line (left panels) and labeled TiS-1 (BT-1). The label TiS+1 (BT) denotes the first oxygen octahedra near the TiS (BT) interface. The bulk value of $\Theta = 167.4$ in $SrTcO_3$ is indicated by the dashed horizontal lines on both figures in the right panel. There, the insets show also the two distinct in-plane angles near the interfaces (solid and dashed lines).

3.2 Interfacial magnetic properties

To illustrate the magnetic properties of the studied $BaTiO_3$–$SrTcO_3$ system, we plot in Fig. 3 the distribution of the Tc magnetic moments m_{Tc} in the subsequent TcO_2 layers calculated within the SwV model. Results for the BT and TiS interfaces and the two opposite polarizations of BTO are shown here. In all cases, the energetically favorable AFM ordering has the G-type, with antiparallel alignment of the nearest Tc moments. In general, the 10%-reduction of the Tc magnetic moments was obtained within a few unit cells of $SrTcO_3$. These magnetic moment changes, which depend on the interface termination and the P-state of BTO, can be viewed as an appearance of the interfacial magnetoelectric coupling. Interestingly, the SL model gives a similar reduction of the Tc magnetic moments, however, this effect is localized within only one unit cell, directly at the interface. This must be a consequence of the confinement effects in the superlattice. Regarding the paraelectric case $P = 0$, the relations between the Tc moments and tilting angles, which are shown in Fig. 2, can be formulated as follows: the closer Θ to 180°, the smaller the magnetic moment. This behavior, which is seen also in our simulations

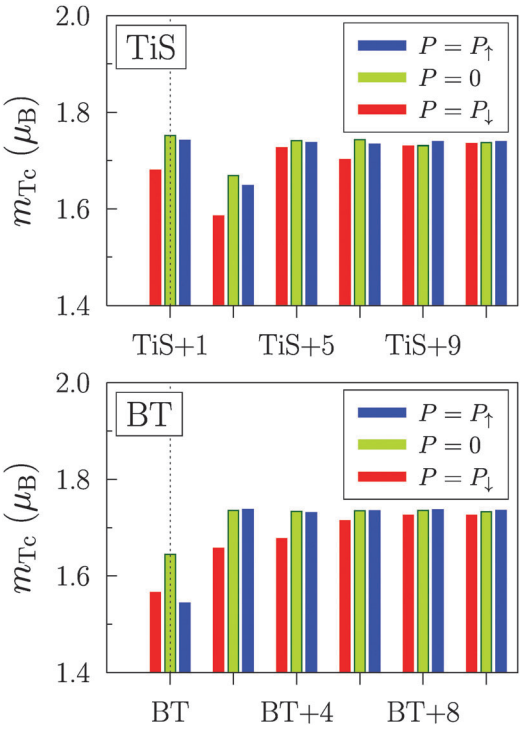

Fig. 3 The layer-resolved magnetic moments of Tc calculated within the SwV model for the three P states, which are presented for each layer by the left (red), middle (green) and right (blue) bars.

of the (001) surface of $SrTcO_3$, is typical for superexchange interaction[38] and can be attributed to the increase of orbital overlap and the consequent electron delocalization as the Tc–O–Tc bond straightens. The dominance of this mechanism in the case of the magnetic $SrTcO_3$ oxide was confirmed by independent studies.[19]

Regarding the magnetic moment induced on Ti near the interfaces, this appears due to orbital hybridization with the nearest (interfacial) O along [001], whose nearest neighbor is Tc along the same chain of atoms: Ti–O–Tc. The Ti moment varies between 0.004 and 0.014 μ_B while the O magnetic moment is larger and varies between 0.02 and 0.08 μ_B depending on the interface composition and polarization of BTO. The two Ti atoms within the same layer are ordered antiferromagnetically to each other and ferromagnetically to both the nearest O and Tc partner along [001]. It should be also noted that the AFM ordering of $ScTcO_3$ induces the alteration of positively and negatively oriented moments within the interfacial Ti–O–Tc chains. When the BTO polarization changes, the magnetic moments of each chain change their values but the total magnetic moment calculated per magnetic supercell is close to zero, varying within $\sum m_i < 10^{-2}$ μ_B. Thus, because of the AFM structure, the magnetoelectric coupling coefficient, α, estimated for the AFM unit-cell interface area is relatively small.

On the other hand, when we consider the BTO unit-cell surface area, which includes a single Ti–O–Tc chain perpendicular to the interface, the change of the total moment, ΔM, becomes valuable. Hence, $\alpha = \Delta M/(E_c \cdot A) > 0$, where A is the surface area of BTO and coercive field $E_c \sim 10$ kV cm^{-1}. For the BT interface, the largest $|\Delta M|$ of 0.12 μ_B is obtained between the $P_\uparrow$-poled and paraelectric BTO, whereas for the TiS interface its largest $|\Delta M| = 0.05$ μ_B corresponds to the switching from $P_\downarrow$ to $P = 0$. The corresponding α varies in the range (1.8–4.0) $\times$ 10^{-10} G cm^2 V^{-1} which is comparable to the values reported for the prototype multiferroic Fe/$BaTiO_3$.[12] In the case of BTO/$SrTcO_3$, it should be kept in mind that both atomic chains couple antiferromagnetically so that their contributions to the total ME effect almost cancel each other.

Studying the system BTO/$SrTcO_3$, one should realize that robust manipulation with the BTO polarization is not obvious. Although the dielectric properties of $SrTcO_3$ have not been reported so far, *ab initio* calculation anticipates that the band gap is significantly smaller[20] than that of BTO. For that reason it is not clear how the coercive field of BTO affects the insulating state of $SrTcO_3$. This issue goes beyond the scope of our theoretical work. Nevertheless, there is always an option to change the BTO polarization, namely, by heating the system above its FE critical temperature of 390 K when BTO becomes paraelectric ($P = 0$) while $SrTcO_3$ remains strongly antiferromagnetic until 1000 K. Thus, the case of $P = 0$ becomes also important when the electronic properties and the 2DEG are discussed.

4 2DEG and the electronic structure

4.1 2DEG

To clarify the 2DEG effect at the BTO/$SrTcO_3$ interface, we calculated the site-projected densities of states (DOS) and obtained the layer-resolved DOS for each termination and for each state of polarization of BTO. The use of the two structural models (Fig. 1) provides the different electrostatic boundary conditions. As each antiferromagnetically ordered oxide layer contains two ABO_3 formula units, the spin contributions were summed up. For the $SrTcO_3$ side, we found that its DOS, $n(E)$, near the Fermi level (E_F) is dominated by the Tc 4d states hybridized with the p states of oxygen. This is similar to the bulk material.[20] However, in the case of BTO/$SrTcO_3$, some oxygen atoms, which are nearest to Tc, belong to polar BTO. As a result, the layer-resolved $n(E)$ near the $SrTcO_3$ interfaces changes significantly compared to the bulk DOS.

For the $P_\downarrow$-state of BTO and for both interfaces (TiS and BT) we obtain $n(E_F) > 0$ while the Fermi level crosses the top of the valence band as shown in Fig. 4. Therefore, the system is not insulating and it should be similar to a p-doped semiconductor with holes as charge carriers. By switching the polarization to $P_\uparrow$ we shift E_F toward the conduction band bottom. Those Tc 4d orbitals which were empty in the bulk material are filled now with electrons and, hence, the n-type charge carriers appear at the interface. For the TiS termination and $P_\uparrow$, the population of the conduction band is smaller compared to the BT termination. Interestingly, such a metallization effect is confined within a few atomic layers near the interface, including the topmost BTO layer whose chemically strong bonds include the neighboring ions of $SrTcO_3$. These bonds show a significant degree of

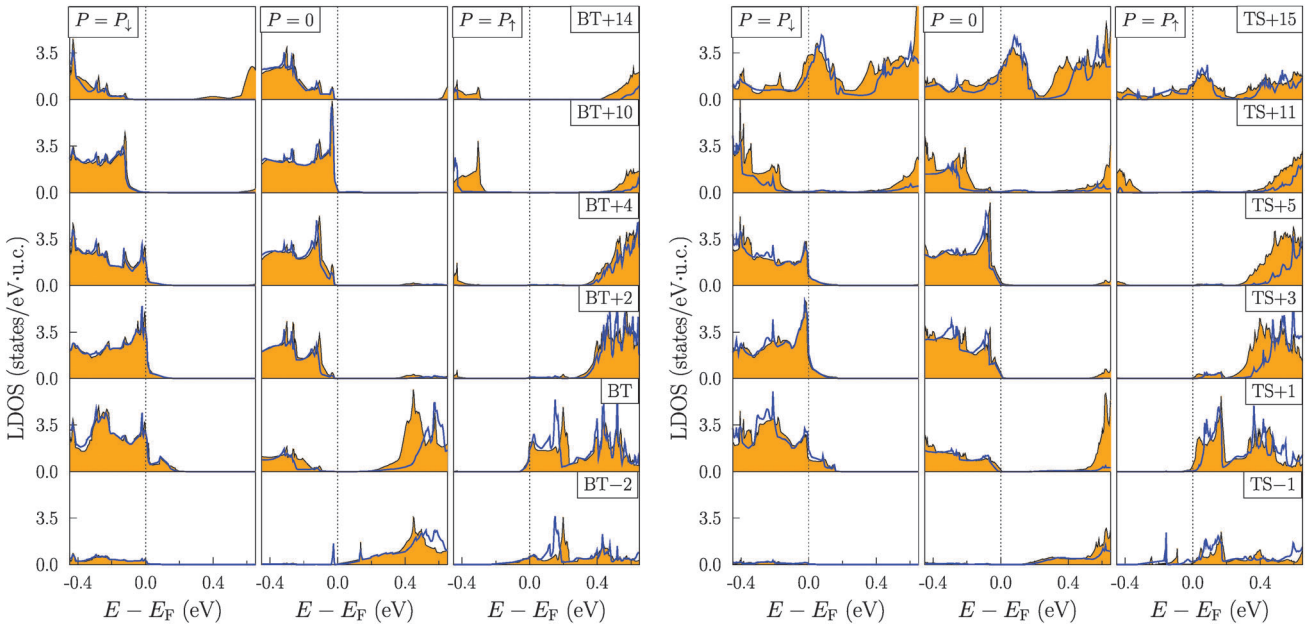

Fig. 4 The total DOS, computed for each ABO_3 unit cell outward the BT (TiS) interface and labeled BT (TS + 1), BT + 2 (TS + 3) *etc.*, are shown in the left (right) panels. Plots at the bottom of each panel represent the interfacial unit cell of the BTO substrate, whereas the plots at the top correspond to the last $SrTcO_3$ unit cell near the (001) surface. For each *P*-state, the site- and orbital-projected contributions were accumulated from the two spin channels. The electronic 4d states of Tc were calculated within the GGA + *U*, and the DOS plotted correspond to $U = 0$ (shaded area) and $U = 0.5$ eV (solid line).

covalency depending on the *P*-state of BTO. A similar effect was obtained also for the superlattice where both interfaces are presented simultaneously. Here, the DOS shift seen in Fig. 6 throughout the whole heterostructure has a slope which is indicative of an electric field induced by the polar BTO in $SrTcO_3$. This leads to the oppositely charged carriers at the two interfaces, *i.e.* if one interface is n-doped the other one becomes p-doped and *vice versa*. The two interfaces are separated by the insulating inner region of $SrTcO_3$ where the response to the BTO polarization is negligible (see, the layer TS + 7 in Fig. 6). However, the electronic states in this inner layer show a pronounced difference from those of the bulk oxide. In particular, the local band gap $E_g' = 0.4$ eV calculated for the inner cell of $SrTcO_3$ is rather small compared to its bulk value of 0.7 eV. In contrast to the SL, the SwV model yields a larger gap for the distant layers from the interface. The above-mentioned differences between the SL and SvW models can be attributed to the specific electrostatic boundary conditions satisfied in each case.

Interestingly, one of our models, namely the SwV model, allows us to include the effect of the free surface on the interfacial 2DEG, which corresponds to a very common experimental setup. For the geometry of our model, we assume that both oxides are grown in complete unit cells. It means that the supercell, which mimics the BT (TiS) interface, has the SrO (TcO_2) termination of $SrTcO_3$(001) and TiO_2 (BaO) termination of BTO(001). Regarding the $SrTcO_3$(001) surface, its SrO-termination appears to be insulating, whereas the TcO_2-terminated free surface is metallic. Layer-by-layer analysis of the electronic states of BTO/$SrTcO_3$(001), which was made outward the surfaces and interfaces, shows that the discussed 2DEG is spatially localized and the chosen supercell was thick enough to simulate the isolated interface. On the other hand, our simulations of the free-standing $SrTcO_3$(001) surface (see, Appendix A) demonstrate that the metallic character is intrinsic to the TcO_2 termination, whereas the insulating SrO termination is energetically favorable and, judging from the local DOS, resembles the bulk material. This difference in the behavior can be attributed to the formation of the interface dipole which screens the potential step at the boundary with vacuum. Band bending, which is a consequence of this dipole, is not sufficient to drive the SrO surface metallic since the conduction band is too far from the Fermi level. However, due to the proximity of the Tc d states to $E = E_F$, which dominate at the TcO_2 surface, band bending effect leads to a strong metallization. In the context of this phenomenon, the geometry suggested for the BT interface with its SrO surface might be preferable for further experimental studies of the 2DEG effect and its applications. Concerning the free surface of BTO in the SwV model of the BT interface, we found it to be insulating for $P = 0$ and $P_\uparrow$ and metallic for $P_\downarrow$. Nevertheless, in the latter case, the second BTO unit cell outward the surface was insulating, which allows retaining the key properties of the ferroelectric material.

The electronic properties of BTO/$SrTcO_3$ may be understood in terms of the bulk electronic states affected by the electric field of BTO, which leads to the band alignment at the interface. In Fig. 5, one can see how the top valence band and the bottom conduction band vary toward the interface for each termination. The upward (downward) shift of the valence (conduction) band above (below) the Fermi level, which is seen for $P_\downarrow$ ($P_\uparrow$), forms the charge carriers distributed predominantly within the 2–3 interfacial cells of $SrTcO_3$. (The SL model makes this region thinner.) In contrast to polar BTO, its paraelectric state prevents the charge transfer and indicates the insulating

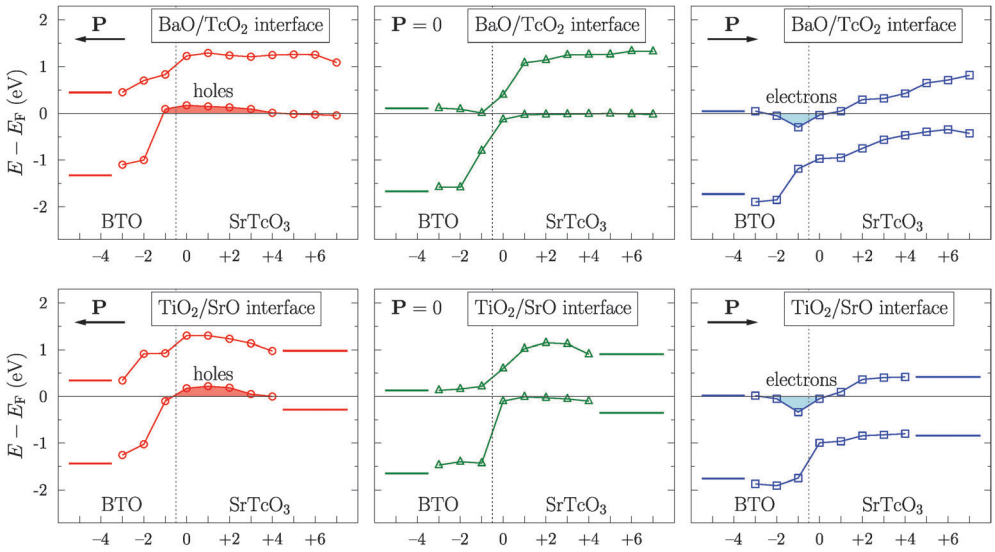

Fig. 5 The layer-resolved energy positions of the top valence and bottom conduction bands with respect to E_F = 0 that are calculated using the SwV model for the three BTO polarizations and differently terminated BTO/$SrTcO_3$ heterostructures. The hole (electron) charge carriers induced in the band gap are shown by red (blue) shaded area. The interface between the two oxides is marked by the vertical dashed line. The asymptotic valence and conduction band edges far from the interface region are shown by solid horizontal lines. The GGA + U results for U = 1.5 eV are shown.

behavior of the system. In the case of $P = 0$, one can also clearly see how the bands flatten away from the interface. The observed difference between the asymptotic valence band boundaries in both materials is due to the different average electrostatic potentials in BTO and $SrTcO_3$. The ratio between this potential step ΔV and the band gaps of both materials is a key factor of the formation of the 2DEG effect. In the studied system, as we see from the middle panels in Fig. 5, these three quantities: the gap width in BTO and $SrTcO_3$, and the potential step ΔV are comparable to each other. It is worth noting that the electrostatic boundary conditions used in our work, although being quite different in their nature, support the scenario of a stable 2DEG. This emphasizes the prominent role of the ferroelectric polarization in this phenomenon. Nevertheless, the detailed picture of the 2DEG should account for the electronic orbital symmetry, spin population and correlation effects for induced charge carriers at the interface.

In view of these results, one can conclude that the character of the 2DEG carriers is changed from electrons to holes upon the **P**-reversal. We estimated and plotted in Fig. 7 the charge, q_i, which is induced in the band gap due to polar BTO and which is accommodated in the ith oxide unit cell near the interfaces. For each P state, the DOS tails seen in the band gap in Fig. 4 and 6 were integrated for each i up to the Fermi level. Although we deal with electrons in all cases, we can formally consider q_i as negative (n-type carriers) when the DOS tail comes from the conduction band and, *vice versa*, $q_i > 0$ (p-type carriers) when the DOS tail comes from the valence band. The corresponding results plotted in the upper panels of Fig. 7 show that the thickness of the region where $|q_i| > 0$ is confined within the 2–3 unit cells near the interface. For the interfacial cell, $|q_i|$ is maximal and then the charge gradually decreases outward the interface.

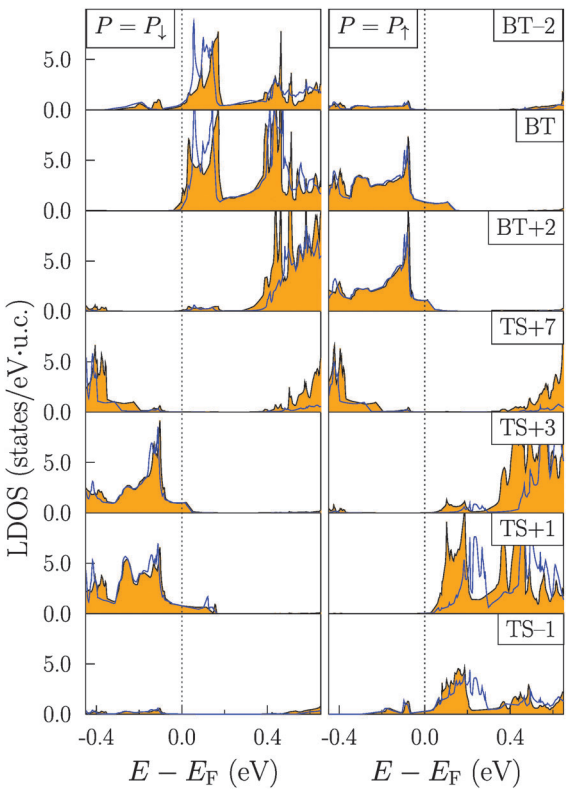

Fig. 6 The total DOS, computed within the superlattice model for the subsequent ABO_3 unit cells and for dually polar BTO ($P_\downarrow$ and $P_\uparrow$). The unit cells are labelled according to their notations in Fig. 1. The lower- and topmost panels represent the interfacial BTO unit cells, while the DOS plotted in the middle panel shows the deep and bulk-like cell of antiferromagnetic $SrTcO_3$. Results within the GGA + U are plotted for U = 0 (shaded area) and U = 0.5 eV (solid line).

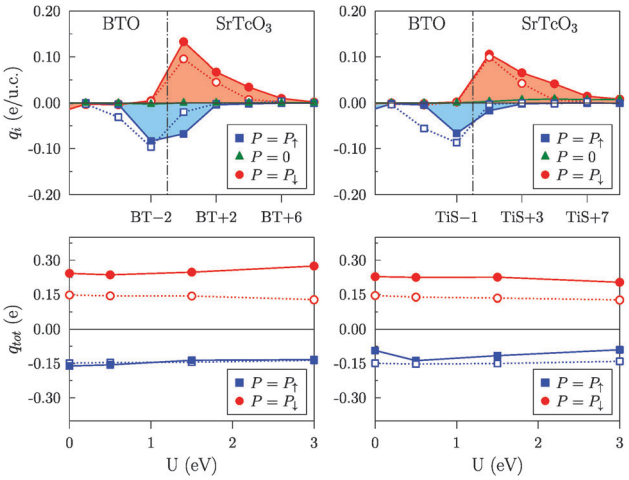

Fig. 7 The charge induced into the band gap by polar BTO and accumulated near the BT (TiS) interface of BTO/$SrTcO_3$. For each unit cell across BTO and $SrTcO_3$ the DOS tails occurring in the gap were integrated. In the upper panels, the results, obtained for $U = 0$ using the two structural models and dually polar BTO, are shown by solid (doted) lines for the SwV (SL) models. Vertical dashed line separates BTO and $SrTcO_3$. In the lower panels, we plot the total charge, induced into the gap and summed over all interfacial layers, as a function of the U parameter.

In the case of $P_\downarrow$, we find hole carries which are mostly localized within the $SrTcO_3$ interfacial region. The $P_\uparrow$ state switches the charge character to electrons while their localization region is shifted towards the BTO side that is seen as the increase of $|q_i|$ in the topmost BTO layers. Quantitatively similar results were obtained using the boundary conditions and electrostatics of the superlattice. For example, the maximal accumulated charge for the $P_\uparrow$-state in both models corresponds to approximately 0.15 electrons. However, the estimated band-gap charge for the $P_\downarrow$-state differs considerably depending on the boundary conditions. Whereas in the superlattice the total charge of the p-type carriers is, disregarding the sign, almost identical to that of the n-type carriers, our calculations in the SwV model reveal a pronounced asymmetry between the carriers of different types. More specifically, the polarization-induced charge near the p-type interface might reach the values of 0.27 electrons, almost by a factor of two larger than at the n-type interface. Another difference between the two models is related to the fact that the charge induced in $SrTcO_3$ is spatially more localized in the superlattice compared to the SwV model. Moreover, the n-type carriers calculated using the SL model are localized almost completely within the BTO side of the system. We attribute this difference to the confinement of the superlattice along [001]. The SwV model and its extra degrees of freedom along [001] distribute the 2DEG spatially. Interestingly, the paraelectric state of BTO results in marginal charges for both terminations of BTO/$SrTcO_3$. Thus, the 2DEG effect appears at the clean and defect-free interface between $SrTcO_3$ and BTO due to ferroelectric BTO. The role of the band gap of $SrTcO_3$ whose width is usually underestimated needs, however, further clarification. This issue will be discussed in Section 4.2.

The tilting of the Tc–O–Tc bonds in bulk $SrTcO_3$ is a key structural feature for its antiferromagnetism. To estimate the total charge q_{tot} induced at BTO/$SrTcO_3$ we used the magnetic-cell surface area. After relaxation, the two pairs of tilted angles are not identical near the interface depending on the polarization and, hence, the type of carriers transferred from BTO. It seems that these flexible bond lengths and angles may support the accumulation of extra charge near the interface. The induced charge was redistributed between several interfacial cations, oxygen atoms and interstitials of $SrTcO_3$ along the chemical bonds. Unfortunately, the charge variations projected on each site are too small to make accurately the corresponding charge analysis.

The electric field which penetrates from BTO into the $SrTcO_3$ side can be traced by analyzing the electrostatic potential energy profile $-eV(z)$ ($e > 0$), calculated along [001], *i.e.* the z axis of the supercell, as shown in Fig. 8. The profile was obtained from the Kohn–Sham effective potential by averaging the VASP outputs over the xy plane within the supercell. The points of the potential profile along [001], which are plotted in Fig. 8 across the BTO/$SrTcO_3$ slab, correspond to the BaO or SrO layers. These results were modeled both for dually polar and for paraelectric BTO. The plotted potentials were calculated within the Hubbard parametrization using $U = 1.5$ eV.

Let us analyze the potential features. Firstly, we see that for any polar BTO side its potential profile shows a remarkable slope, the sign of which changes upon the **P**-reversal, as expected from electrostatics. Near the interface, the picture becomes complicated because of the depolarizing field $\vec{E}_{depol}$, which acts against the intrinsic polarization of BTO. In the paraelectric case ($P = 0$), there is a small slope of the potential, which persists in the interfacial BTO cells due to the structural displacements discussed above (see Fig. 2). The first two cells of $SrTcO_3$ near the interface exhibit similar structural displacements seen in Fig. 2 and, therefore, the polarization is locally

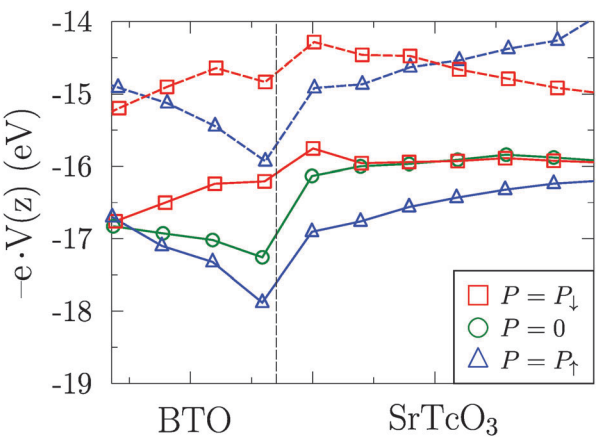

Fig. 8 The electrostatic potential profile along [001], which was calculated for the BT-terminated interface of BTO/$SrTcO_3$ using the supercell in a vacuum (solid lines) and the superlattice model (dashed lines). Each point plotted corresponds to the BaO or SrO layers while the interface is shown by the vertical dashed line. Dually polar and paraelectric BTO were modeled. The negative charge of electrons was included.

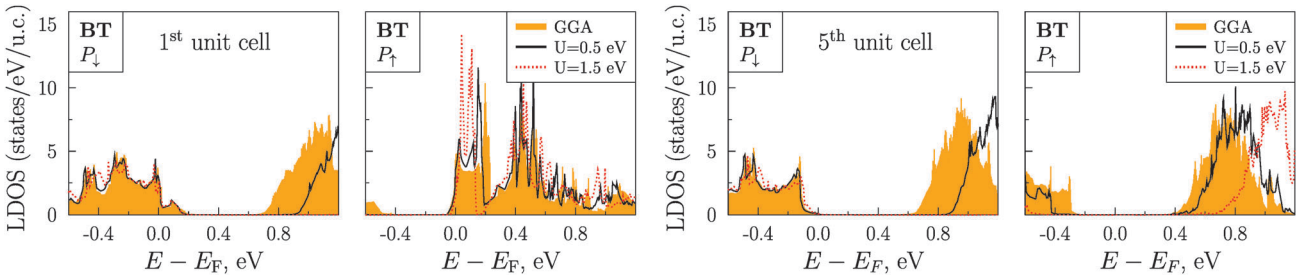

Fig. 9 The DOS curves of the first (fifth) $SrTcO_3$ cell counting from the polar BT interface are plotted in the two left (right) panels for $P_\downarrow$ and $P_\uparrow$. The SwV model was used there. The U = 0 option is shown by shaded area and the results for U = 0.5 eV and U = 1.5 eV are shown by the solid and dashed lines, respectively.

induced even if the BTO side is paraelectric. The continuity condition for $\vec{D}$ is fulfilled also in this particular case, so that $\vec{D}_1 = \vec{E}_{depol}$ in BTO and $\vec{D}_2 = 4\pi\vec{P}_{ind}$ in $SrTcO_3$ are equal to each other at the interface. As a result, non-zero depolarizing field $\vec{E}_{depol}$ is present in the BTO side, which is illustrated by the potential profile for P = 0 in Fig. 8.

The results shown in Fig. 8 for the supercell with vacuum indicate that the local potential in $SrTcO_3$ is flat far away from the interface. In the case of $P_\downarrow$, *i.e.* when the hole carriers were induced in $SrTcO_3$, the potential slope in BTO is positive and, as a result, the potential adjustment goes smoothly. For P = 0, the "artificial" slope near the interface, from its BTO side, is modestly negative, which results in a downward shift of the potential in the first $SrTcO_3$ layer and, then, outwards the interface the $SrTcO_3$ potential quickly approaches its bulk value. In the case of $P_\uparrow$, the local shift of the potential at the interface is about 1 eV. As a result, the electric field of BTO penetrates deeply into the $SrTcO_3$ side and a few more atomic layers are needed to screen this field and to flatten the potential profile. The electrostatic potential in the superlattice (dashed lines in Fig. 8) is characterized by similar slopes near the interfaces. For the SwV model, however, the shift seen in the potential profile across the interface is not so dramatic compared to the free surface. It should be noted that near each (001) surface of the slab the potential profile exhibits a polar discontinuity widely discussed in the literature,[39] whereas the potential in the vacuum goes to zero ($V(z) \to 0$) when the dipole corrections are applied.[40]

Paraelectric BTO provides an extra option. For P = 0, there is no field which needs to be screened. Indeed, by inspecting the DOS calculated for the two terminations we see that the interface is insulating, as shown in Fig. 4. However, there are only some marginal and spatially extended charges seen in Fig. 7, which appear after structural relaxations. When the 4d electrons of Tc are treated as strongly correlated the insulating behavior of the studied multiferroic system enhances, since the band gap of $SrTcO_3$ widens. In practice, the paraelectric state of BTO can be obtained by heating the system above the T_C of BTO and keeping the temperature below the Néel temperature of $SrTcO_3$. This suggests another scenario of a thermally switchable 2DEG in BTO/$SrTcO_3$, which differs from that of the **P**-reversal in BTO. The polarization reversal switches the 2DEG charge carries from electrons to holes. In contrast, thermally the 2DEG can be switched on and off.

To gain a better insight into the band structure of BTO/$SrTcO_3$(001) and to show how the electronic states depend on the BTO polarization, we plot in Fig. 10 the dispersion curves, $E(\vec{k}_\parallel)$, as a function of the in-plane $\vec{k}_\parallel$-vector along the $\bar{\Gamma}$–$\bar{X}$ direction in the quasi-two-dimensional Brillouin zone. Here, we analyzed the Tc-projected contributions of each 4d orbital and found that the spin majority d_{xz}/d_{yz} and $d_{x^2-y^2}$ orbitals of Tc (the majority and minority channels were defined in accordance with the sign of the local magnetic moment) are responsible for the hole character of the 2DEG both at the TiS and the BT interfaces calculated for the $P_\downarrow$-state of BTO. This is in accordance with the mechanism proposed to explain the formation of the 2DEG. In bulk $SrTcO_3$, the top of the valence band is formed by the strongly spin-polarized (>90%) 4d states of Tc hybridized with the ligand p states. In BTO/$SrTcO_3$, the $P_\downarrow$-poled BTO induces positively charged holes in the topmost layers of $SrTcO_3$. One can see that in Fig. 10. After switching the

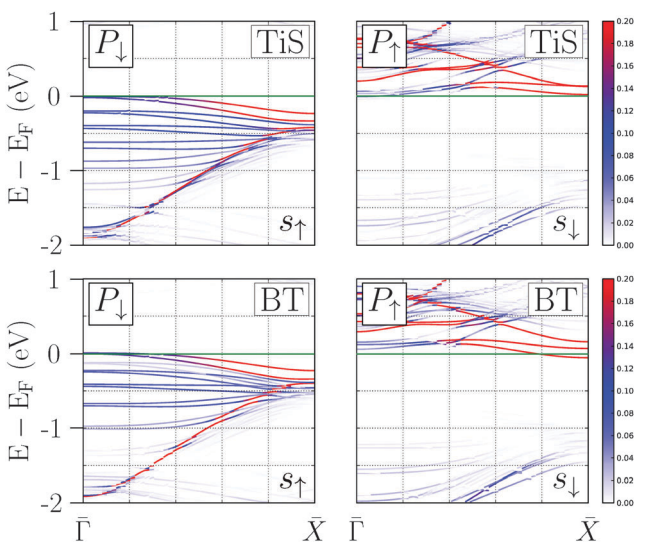

Fig. 10 The quasi-two-dimensional band structure calculated for the interfaces BT and TiS and dually poled BTO: $P_\downarrow$ (left panels) and $P_\uparrow$ (right panels). The dispersion curves $E_n(\vec{k}_\parallel)$, which contribute to the DOS at $E = E_F$, are plotted along the $\bar{\Gamma}$–$\bar{X}$ in-plane direction of the 2D Brillouin zone. We plot the bands $E_n(\vec{k}_\parallel)$ with the significant partial charge of the Tc 4d spin-up (for $P_\downarrow$) or spin-down (for $P_\uparrow$) states using the colored curves, where red corresponds to the largest partial charge. The GGA + U results for U = 0.5 eV are shown.

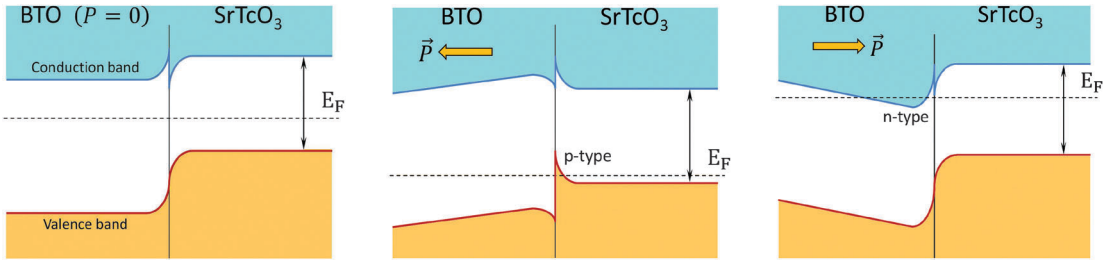

Fig. 11 Sketch of the band alignment and their bending at the BTO/$SrTcO_3$(001) interface with dually polar and paraelectric BTO side.

polarization direction to $P_\uparrow$, the carriers induced in $SrTcO_3$ become negatively charged, namely, electrons which populate the bottom of the conduction band. In insulating bulk $SrTcO_3$ its lowest empty band is formed by the spin minority states of the d_{xz}/d_{yz} and $d_{x^2-y^2}$ orbitals. Near the interface, however, the $d_{x^2-y^2}$ states are shifted away from $E = E_F$ towards higher energies, so that only the d_{xz}/d_{yz} states can be populated there. In all cases, the Tc-projected d bands crossing the Fermi level are relatively flat, which may point out their abnormal electronic correlations.

To summarize this part, a robust 2DEG effect is expected at the two specifically terminated, defect-free and atomically sharp BTO/$SrTcO_3$ interfaces. The effect might be controlled by the ferroelectric state of the BTO substrate. Based on our findings, we conclude that the electronic properties of the studied interface are governed by the induced charge carriers whose sign changes upon the polarization reversal in BTO. The suppression of polarization in BTO to its paraelectric state destroys the 2DEG. The specific structural tilting and the AFM ordering in $SrTcO_3$, which are responsible for its modest insulating band gap, support charge accumulation in this magnetic oxide and the formation of the 2DEG, although the major role is played by the ferroelectric BTO. The electronic properties of BTO/$SrTcO_3$ may be understood in terms of the bulk electronic states affected by the electric field of BTO, which leads to the band alignment at the interface. In Fig. 11, the mechanism of this phenomenon is sketched in a similar fashion, as usually done for semiconducting heterostructures. In the absence of polarization in BTO, the interface dipole dominates the band alignment. However, due to specific relations between the band gaps and the potential step at the interface, the 2DEG is not formed in this case. The non-zero BTO polarization is solely responsible for the additional shift of the valence/conduction bands which follow the trend shown already in Fig. 8 and results in a local depletion or occupation of the involved states. The model diagrams in Fig. 11 help us to understand issues such as the type of carriers and their localization at the interface as a function of the BTO polarization state.

4.2 Effects of electronic correlations

In our study of bulk $SrTcO_3$ within the GGA + U parametrization, it has been pointed out that a relatively small U parameter is needed to improve the calculated magnetic properties, in particular, the local moments and the Néel temperature.[20] In this work, we analyzed the influence of electronic correlations on the 2DEG of BTO/$SrTcO_3$ using the same approach. By comparing the corresponding DOS with that of $U = 0$, both of which are shown in Fig. 4, 6 and 9, we demonstrate how the degree of electronic correlations affects the Tc d states and the entire band picture.

The main effect of U is the band gap widening. This is similar to what we found previously for bulk $SrTcO_3$.[20] The gap widening is clearly seen in the layer-resolved DOS. For instance, the DOS corresponding to the fifth $SrTcO_3$ unit cell from the interface is very similar to that of the bulk material. Upon increasing U up to 3 eV, the band gap increases by almost a factor of three compared to the gap of $U = 0$. This agrees well with our bulk calculation where the gap value increases from 0.7 eV computed for $U = 0$ to 1.8 eV for $U = 3$ eV.

By inspecting the total charge q_{tot} accumulated at the interface, which is plotted in the two lower panels of Fig. 7, we found that both types of chemically different interfaces support the formation of a 2DEG which experiences only marginal impact from electronic correlations. In both studied models, the value of charge q_{tot} related to the 2DEG changes by less than 0.05 electrons as the U parameter varies in the chosen range (0–3) eV, far above its optimal value for $SrTcO_3$.[20] The robustness of the considered 2DEG phenomenon can be perceived from the evolution of the site-projected density of states as a function of the U parameter (two cases $U = 0$ and 0.5 eV are presented in Fig. 4 and 6). Our calculations for the p-type interface show that the energy position of bands crossing the Fermi level, thereby forming the hole-type 2DEG, is stable with respect to the U variations. On the other hand, the correlations near the n-type interface push the DOS peaks from the Fermi level towards higher energies. Despite this fact, the 2D electron gas is not weakened but simply redistributed towards the BTO side, where it is accommodated by the Ti d states. For larger U values, the 2DEG is mostly localized within the interfacial BTO cells. This observation suggests that the induced holes in the studied oxide system are less sensitive to electronic correlations than the induced electrons. Regarding the paraelectric state of BTO, for which the interface seems to be insulating, we suggest that strong electronic correlations enhance the insulating properties due to the larger band gap of the $SrTcO_3$ side for larger U values.

Equally important is the influence of the BTO band gap E_g on the 2DEG density. We applied the GGA + U scheme on the Ti d states in order to improve the description of the conduction

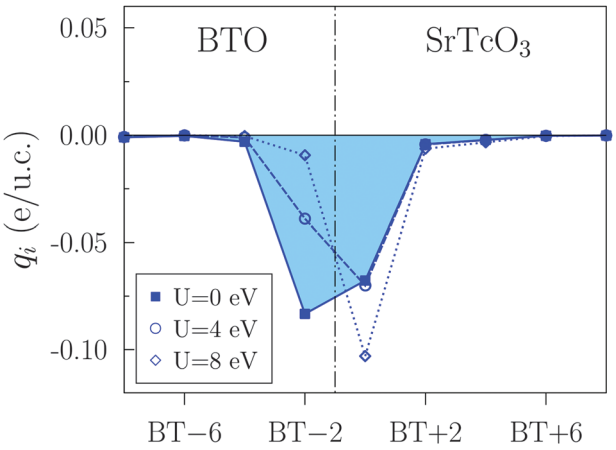

Fig. 12 The layer-resolved band-gap charge distribution for the BT type of interface with the $P_\uparrow$ polarization of BTO. Electronic correlations on the Ti d states are taken into account using the GGA + U scheme with U = 0, 4 and 8 eV.

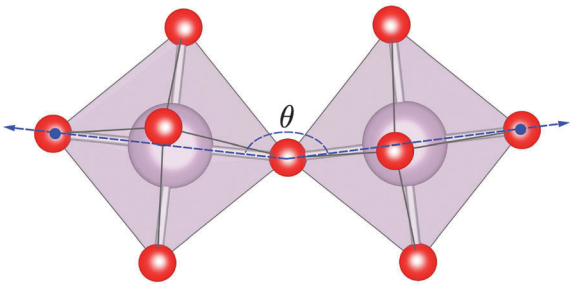

Fig. 13 Distorted oxygen octahedra of bulk $SrTcO_3$. The tilting is characterized by the angle θ between the equatorial planes of the neighboring octahedra.

band position. For the studied range of values U = (0–8) eV, we obtained an increase of E_g in the bulk material from 1.8 eV to 2.8 eV, which is close to the experimental value (3.2 eV). Under these conditions, the charge induced into the band gap of BTO, which is a part of the discussed 2DEG, becomes gradually expelled from the ferroelectric material and, for U = 8 eV, it resides predominantly in $SrTcO_3$ (Fig. 12). Since large values of U are not expected for the latter, the 2DEG behavior remains stable and localizes within the material with a smaller band gap ($SrTcO_3$ in this case), which is intuitive in view of the band alignment effects shown in Fig. 11.

5 Conclusions

In summary, we presented *ab initio* calculations of the structural, magnetic and electronic properties of differently terminated interfaces between a typical ferroelectric $BaTiO_3$ and strongly antiferromagnetic perovskite $SrTcO_3$. Interfacial cation intermixing and the presence of steps, oxygen vacancies and extra species, such as O or C, were excluded. To study the BTO/$SrTcO_3$ interfaces we used the two structural models which mimic the electrostatic boundary conditions differently: (i) the supercell with one specifically terminated interface and a vacuum layer (SwV) separating the oxide surfaces, and (ii) the superlattice (SL) in which both interfacial terminations are presented simultaneously. We assumed that each oxide in $BaTiO_3/SrTcO_3$ was grown in complete unit cells along [001]. For each structural model, the spin-polarized DOS projected on all interfacial species were calculated in response to the three polarization states of BTO, including paraelectric (P = 0).

The most important effect of polar BTO is the formation of a 2DEG for which the charge character of induced carriers can be switched from the p- to n-type by polarization reversal. The dominant mechanism of the 2DEG effect at BTO/$SrTcO_3$ is the electron/hole charge transfer across the interface induced by the polar BTO, so that the charge carries are accumulated near the interface within a few atomic layers. When BTO is paraelectric the 2DEG disappears, indeed. There is another important factor needed to create the 2DEG conditions: a modest band-gap width of $SrTcO_3$ (less than 1.5 eV) which allows the band bending effect seen as sufficiently shifted electronic states. For an abnormally large gap of $SrTcO_3$ we anticipate that one of the two interface terminations could become completely insulating while for the other one the 2DEG may be conserved for $P_\downarrow$ only. A variety of boundary conditions considered in our work suggest that the 2DEG is stable and its spatial distribution diminishes in the heterostructure modeled as a superlattice. It would be worthwhile to inspect the interface between two semi-infinite oxides.

The tilting of oxygen octahedra and related AFM ordering in $SrTcO_3$, which support the insulating bulk properties, might also contribute to the 2DEG effect. The charge induced from polar BTO is redistributed between several interfacial cations, oxygens and interstitials of $SrTcO_3$ along the chemical bonds. Here, the tilting angles and the bond lengths seem to be rather flexible to accommodate all excessive charges of both characters. For the BaO/TcO_2 termination, because of its interfacial Tc and flexible tilting, we found that the 2DEG effect is more pronounced and stable with respect to the model variations, such as the film thickness, boundary conditions and degree of electronic correlations. This opens up an opportunity to control the transport properties of $BaTiO_3/SrTcO_3$ either by switching the polarization state of BTO or alternatively by heating the system above the FE transition temperature to the paraelectric state which suppresses the 2DEG.

It should be noted that both oxides studied here are assumed to grow in complete unit cells. Since the surface termination and interfacial composition are correlated, then, using some appropriate bottom termination of the substrate, the target BaO/TcO_2 termination and, hence, the 2DEG can be designed. So far, the 2DEG effect was reported for the TiO_2/LaO termination of $LaAlO_3/SrTiO_3$.[1] This 2DEG is formed by paraelectric and paramagnetic oxides and, therefore, it is not externally switchable. Now we suggest that the controlled 2DEG may appear at the BTO/$SrTcO_3$ interface. The anticipated 2DEG is localized within the few-nm-thick layer. Since the 2DEG effect is ferroelectrically driven, it can be (i) switched off completely by heating or (ii) adjusted from the hole-type carriers to electrons by the

P-reversal of BTO. This offers further promising applications. Unfortunately, we are not able to suggest the voltage needed for the **P**-reversal. It is also difficult to claim which polarization state, either $P_{\downarrow}$ or $P_{\uparrow}$, is initially formed under the non-equilibrium growth conditions. The energetics in our study is based on the total energy calculations at zero temperature while all finite-temperature contributions to the free energy, such as vibrational energy, entropy and anharmonic terms, were excluded. These can shift the balance to a polarization pattern different from the ground state.[41] Our findings could stimulate further theoretical studies, which include the effect of spin–orbit coupling on spin dynamics in non-centrosymmetric composite oxides.[42]

Appendix A: $SrTcO_3$(001) surface

For $SrTcO_3$(001), we studied which termination, either TcO_2 or SrO, is energetically preferable. It is also necessary to elucidate how the magnetic structure near the surface depends on the termination. The slab, which simulates the dually terminated free (001)-surface of $SrTcO_3$, contains 14 monolayers (ML) with two Tc per each TcO_2 ML. The supercell corresponds to the thickness of 7 conventional ABO_3 unit cells along [001]. The lattice parameters are $a = b = \sqrt{2}a_0 \times \sqrt{2}a_0$ and $c = 2a_0$, where a_0 = 3.976 Å is the equilibrium Tc–Tc distance in the bulk material. A vacuum of about 20 Å is added to ensure that there is no interaction between the opposite surfaces. The four topmost MLs near the surface (2 unit cells) were completely relaxed. For the surface-energy calculation we used the procedure described previously for $BaTiO_3$(001).[36,43]

By comparing the two sets of calculation for dually terminated $SrTcO_3$(001) we found that the SrO termination is energetically favorable by 0.04 eV per $\sqrt{2}a_0 \times \sqrt{2}a_0$ surface area, as compared to the TcO_2 termination. The lower energy of the SrO-terminated surface can be accounted for by the formation of the surface dipole which screens the large potential step on the vacuum side and simultaneously leads to the band bending effect. The latter can become particularly strong, so that the conduction band is locally occupied, which happens in our simulations of the TcO_2 surface. This indicates that the potential step is larger for the TcO_2-terminated surface, which is, in this respect, unfavourable compared to SrO.

The charge-density cuts along the (010) plane of $SrTcO_3$(001), which are plotted in Fig. 14 for each termination, may clearly illustrate the relaxation process. The x–z plane cut was chosen because it shows the altering O–Tc–O angle along the z axis, whereas the y–z plane has $\Theta = 180^\circ$ along [00z].

Interestingly, the flatter Θ near the surface, the more distorted is the SrO layer. The O–Sr–O angle is shown in Fig. 14 by the dashed line. For the SrO termination, the O atoms relax above Sr by 0.25 Å.

The angle Θ and its variation near the surface can characterize the oxygen octahedra tilting in the system. In the text below, the topmost surface ML of $SrTcO_3$(001) is denoted S while the layers outward the surface are labeled S-1, S-2 and so on. Fig. 15 shows

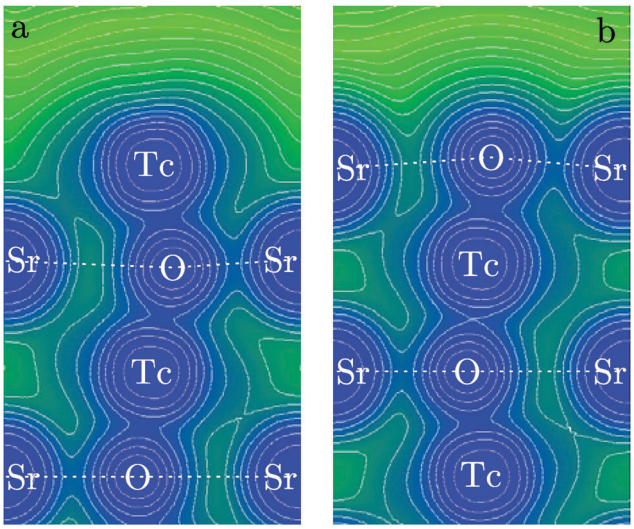

Fig. 14 Cut in the x–z plane of the charge density distribution calculated for the top four layers of $SrTcO_3$(001). The two surface terminations: TcO_2 (a) and SrO (b) are shown.

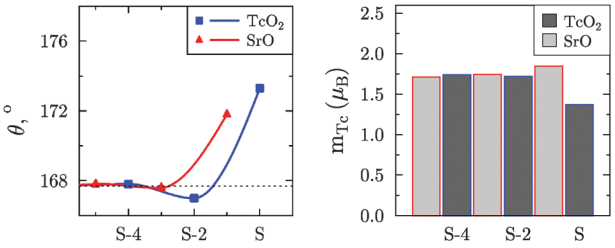

Fig. 15 The tilting angle, Θ, calculated for the dually terminated $SrTcO_3$(001) surface, is plotted in the left panel *vs.* the TcO_2-layer position toward the surface S. In the right panel, the Tc magnetic moments are plotted for each termination as a function of the TcO_2-layer position.

that Θ increases in the ML S from its bulk value to 173.3° (171.8°) for the TcO_2 (SrO) termination.

For the TcO_2 termination, the Tc magnetic moment in layer S decreases by 20% from its bulk value of 1.73 μ_B to 1.37 μ_B. For the SrO-terminated surface m_{Tc} in the layer S-1 slightly increases to 1.85 μ_B compared to the bulk magnetic moment. The reduction of m_{Tc} for the topmost ML S is in a good agreement with the moment in the cubic-structure $SrTcO_3$ where $\Theta = 180^\circ$.[20]

In Fig. 16, we plot the DOS calculated for dually terminated $SrTcO_3$(001). Since both spin channels were included, the surface area of one formula unit was used. Each DOS curve was obtained by summing up the local DOS at one Sr, one Tc and three O sites of the two top monolayers S and S-1. The DOS contribution from Tc is shown in Fig. 16 by the shaded area. The corresponding DOS of bulk $SrTcO_3$ is also plotted for comparison in the top panel of Fig. 16. For the SrO-terminated surface, its DOS differs insignificantly from that of the bulk DOS, whereas the TcO_2 termination causes metallic behavior of the topmost ML. In this case, the Tc d states mostly form the DOS feature near the Fermi level.

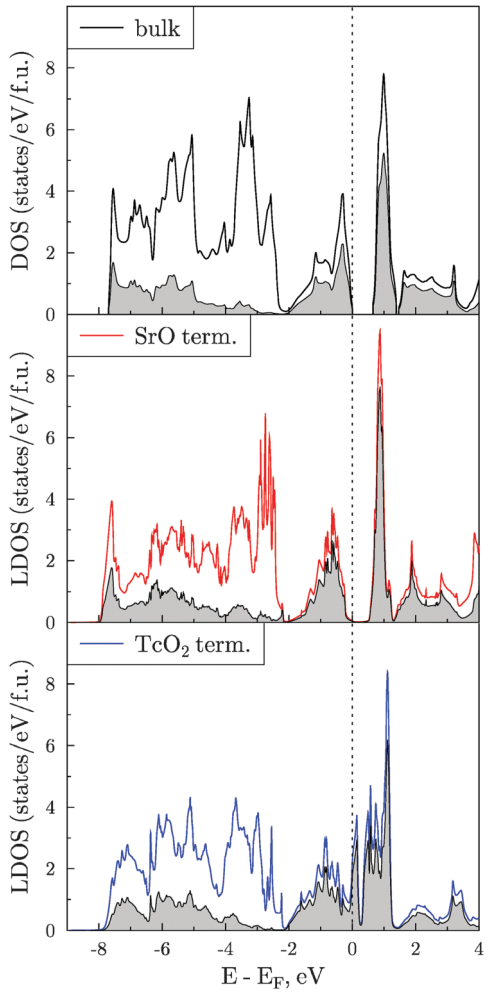

Fig. 16 Density of states of the SrO- and TcO_2-terminated surfaces of $SrTcO_3$(001) in comparison with the DOS of the bulk material. Each DOS of $SrTcO_3$(001) was obtained by summing up the local DOS projected on the Sr, Tc and three O sites of the two top monolayers S and S-1. The contribution of the technetium d states is shown by the shaded areas.

Acknowledgements

We would like to thank Francisco Muñoz for kindly providing the PyProcar code (http://sourceforge.net/projects/pyprocar) which was used during the post-processing of the computed band structure and for preparing the corresponding figures. We are also thankful to Marin Alexe for fruitful discussions. This work was supported by Sonderforschungsbereich SFB 762, 'Functionality of Oxide Interfaces'.

References

1 A. Ohtomo and H. Y. Hwang, *Nature*, 2004, **427**, 423–426.
2 S. Thiel, G. Hammerl, A. Schmehl, C. W. Schneider and J. Mannhart, *Science*, 2006, **313**, 1942–1945.
3 N. Nakagawa, H. Y. Hwang and D. A. Muller, *Nat. Mater.*, 2006, **5**, 204–209.
4 H. Y. Hwang, Y. Iwasa, M. Kawasaki, B. Keimer, N. Nagaosa and Y. Tokura, *Nat. Mater.*, 2012, **11**, 103–113.
5 N. Pavlenko, T. Kopp, E. Y. Tsymbal, J. Mannhart and G. A. Sawatzky, *Phys. Rev. B: Condens. Matter Mater. Phys.*, 2012, **86**, 064431.
6 V. Vonk, J. Huijben, D. Kukuruznyak, A. Stierle, H. Hilgenkamp, A. Brinkman and S. Harkema, *Phys. Rev. B: Condens. Matter Mater. Phys.*, 2012, **85**, 045401.
7 R. Pentcheva and W. E. Pickett, *J. Phys.: Condens. Matter*, 2010, **22**, 043001.
8 G. Herranz, F. Sánchez, N. Dix, M. Scigaj and J. Fontcuberta, *Sci. Rep.*, 2012, **2**, 758.
9 S. C. Chae, W. S. Choi, H. K. Yoo and B. S. Kang, *Curr. Appl. Phys.*, 2011, **11**, 521–524.
10 J. Junquera and P. Ghosez, *Nature*, 2003, **422**, 506–509.
11 M. Stengel, P. Aguado-Puente, N. A. Spaldin and J. Junquera, *Phys. Rev. B: Condens. Matter Mater. Phys.*, 2011, **83**, 235112.
12 C. G. Duan, S. S. Jaswal and E. Y. Tsymbal, *Phys. Rev. Lett.*, 2006, **97**, 047201.
13 D. I. Khomskii, *J. Magn. Magn. Mater.*, 2006, **306**, 1–8.
14 Y. Wang, M. K. Niranjan, J. D. Burton, J. M. An, K. D. Belashchenko and E. Y. Tsymbal, *Phys. Rev. B: Condens. Matter Mater. Phys.*, 2009, **79**, 212408.
15 J. B. Goodenough, *Rep. Prog. Phys.*, 2004, **67**, 1915.
16 T. Wolfram and S. Ellialtioglu, *Electronic and Optical Properties of d-Band Perovskites*, Cambridge University Press, Cambridge, 2006.
17 E. E. Rodriguez, F. Poineau, A. Llobet, B. J. Kennedy, M. Avdeev, G. J. Thorogood, M. L. Carter, R. Seshadri, D. J. Singh and A. K. Cheetham, *Phys. Rev. Lett.*, 2011, **106**, 067201.
18 M. Avdeev, G. J. Thorogood, M. L. Carter, B. J. Kennedy, J. Ting, D. J. Singh and K. S. Wallwork, *J. Am. Chem. Soc.*, 2011, **133**, 1654–1657.
19 C. Franchini, T. Archer, J. He, X.-Q. Chen, A. Filippetti and S. Sanvito, *Phys. Rev. B: Condens. Matter Mater. Phys.*, 2011, **83**, 220402.
20 V. S. Borisov, I. V. Maznichenko, D. Böttcher, S. Ostanin, A. Ernst, J. Henk and I. Mertig, *Phys. Rev. B: Condens. Matter Mater. Phys.*, 2012, **85**, 134410.
21 G. Kresse and J. Hafner, *Phys. Rev. B: Condens. Matter Mater. Phys.*, 1994, **49**, 14251–14269.
22 G. Kresse and J. Furthmüller, *Phys. Rev. B: Condens. Matter Mater. Phys.*, 1996, **54**, 11169–11186.
23 J. Hafner, *J. Comput. Chem.*, 2008, **29**, 2044–2078.
24 J. P. Perdew, K. Burke and M. Ernzerhof, *Phys. Rev. Lett.*, 1996, **77**, 3865–3868.
25 P. E. Blochl, *Phys. Rev. B: Condens. Matter Mater. Phys.*, 1994, **50**, 17953–17979.
26 H. J. Monkhorst and J. D. Pack, *Phys. Rev. B: Solid State*, 1976, **13**, 5188–5192.
27 S. L. Dudarev, G. A. Botton, S. Y. Savrasov, C. J. Humphreys and A. P. Sutton, *Phys. Rev. B: Condens. Matter Mater. Phys.*, 1998, **57**, 1505–1509.
28 R. Pentcheva, R. Arras, K. Otte, V. G. Ruiz and W. E. Pickett, *Philos. Trans. R. Soc., A*, 2012, **370**, 4904–4926.
29 H. L. Meyerheim, F. Klimenta, A. Ernst, K. Mohseni, S. Ostanin, M. Fechner, S. Parihar, I. V. Maznichenko, I. Mertig and J. Kirschner, *Phys. Rev. Lett.*, 2011, **106**, 087203.

30 D. J. Kim, H. Lu, S. Ryu, C.-W. Bark, C.-B. Eom, E. Y. Tsymbal and A. Gruverman, *Nano Lett.*, 2012, **12**, 5697–5702.
31 H. L. Meyerheim, A. Ernst, K. Mohseni, I. V. Maznichenko, J. Henk, S. Ostanin, N. Jedrecy, F. Klimenta, J. Zegenhagen, C. Schlueter, I. Mertig and J. Kirschner, *Phys. Rev. Lett.*, 2013, **111**, 105501.
32 M. Stengel and N. A. Spaldin, *Nature*, 2006, **443**, 679–682.
33 N. Sai, C. J. Fennie and A. A. Demkov, *Phys. Rev. Lett.*, 2009, **102**, 107601.
34 N. A. Benedek and C. J. Fennie, *Phys. Rev. Lett.*, 2011, **106**, 107204.
35 M. Stengel, C. J. Fennie and P. Ghosez, *Phys. Rev. B: Condens. Matter Mater. Phys.*, 2012, **86**, 094112.
36 M. Fechner, S. Ostanin and I. Mertig, *Phys. Rev. B: Condens. Matter Mater. Phys.*, 2008, **77**, 094112.
37 A. Y. Borisevich, H. J. Chang, M. Huijben, M. P. Oxley, S. Okamoto, M. K. Niranjan, J. D. Burton, E. Y. Tsymbal, Y. H. Chu, P. Yu, R. Ramesh, S. V. Kalinin and S. J. Pennycook, *Phys. Rev. Lett.*, 2010, **105**, 087204.
38 P. W. Anderson, *Phys. Rev.*, 1959, **115**, 2–13.
39 M. Stengel and D. Vanderbilt, *Phys. Rev. B: Condens. Matter Mater. Phys.*, 2009, **80**, 241103.
40 L. Bengtsson, *Phys. Rev. B: Condens. Matter Mater. Phys.*, 1999, **59**, 12301–12304.
41 A. Höfer, M. Fechner, K. Duncker, M. Hölzer, I. Mertig and W. Widdra, *Phys. Rev. Lett.*, 2012, **108**, 087602.
42 C. Şahin, G. Vignale and M. E. Flatté, *Phys. Rev. B: Condens. Matter Mater. Phys.*, 2014, **89**, 155402.
43 R. I. Eglitis and D. Vanderbilt, *Phys. Rev. B: Condens. Matter Mater. Phys.*, 2007, **76**, 155439.